Inorganic Chemistry

including bioinorganic chemistry

June 2, 2014
Volume 53, Number 11
pubs.acs.org/IC

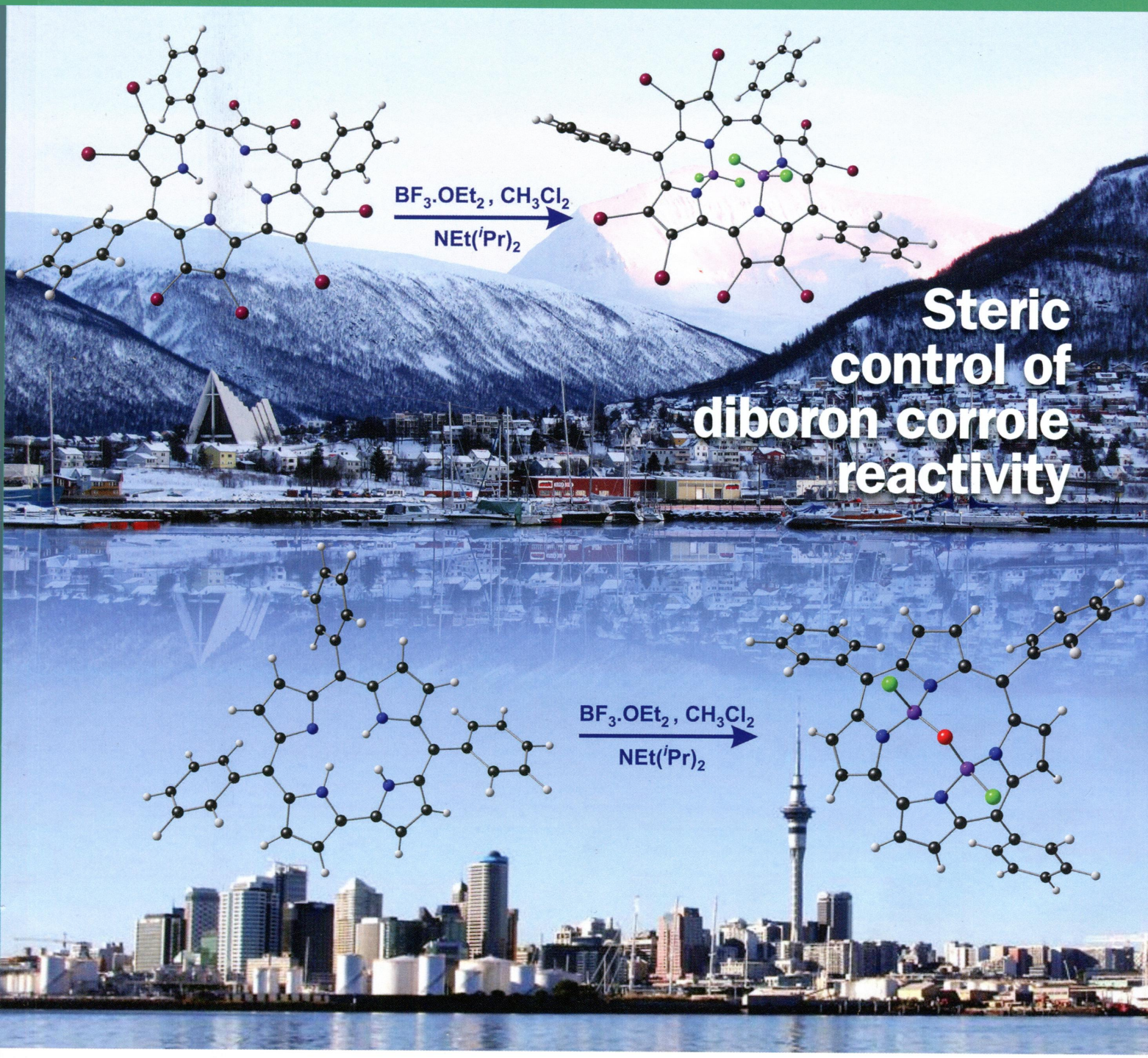

ACS Publications
Most Trusted. Most Cited. Most Read.

www.acs.org

Inorganic Chemistry

JUNE 2, 2014
VOLUME 53 ISSUE 11

INOCAJ 53(11) 5405–5874 (2014)
ISSN 0020-1669

ON THE COVER: In the Arctic, the reaction of free base corrole with BF_3 produces a transoid diboryl corrole complex (top), but the same reaction in the South Pacific gives a dome-shaped, cisoid FBOBF corrole complex (bottom). The difference arises because the more highly substituted octabromotriarylcorrole (top) inhibits the domed deformation and, hence, the hydrolysis reaction. Cover art by M. M. Conradie and J. Conradie. See A. M. Albrett, K. E. Thomas, S. Maslek, A. Młodzianowska, J. Conradie, C. M. Beavers, A. Ghosh, and P. J. Brothers, p 5486.

Communications

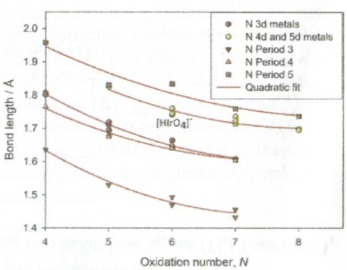

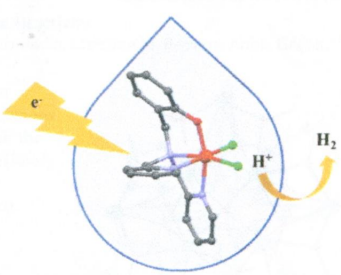

5411 S dx.doi.org/10.1021/ic500474j

Zeolitic Imidazolate Framework as Formaldehyde Gas Sensor

Er-Xia Chen, Hui Yang, and Jian Zhang*

ZIF-67 (surface area of 1832.2 $m^2\ g^{-1}$) was first employed as a promising formaldehyde gas sensor at a low operating temperature (150 °C).

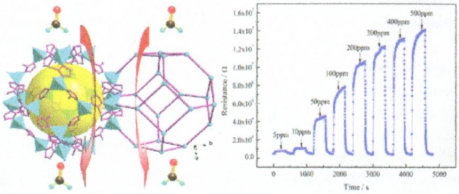

5414 S dx.doi.org/10.1021/ic500558j

Highest Recorded N–O Stretching Frequency for 6-Coordinate {Fe-NO}^{7} Complexes: An Iron Nitrosyl Model for His$_3$ Active Sites

Jia Li, Atanu Banerjee, Piotr L. Pawlak, William W. Brennessel, and Ferman A. Chavez*

Herein we report the synthesis and structure of a model complex for His$_3$ nonheme enzyme active sites. The 5-coordinate iron(II) complex features three imidazolyl ligands. The reaction of this compound with nitric oxide affords a 6-coordinate {FeNO}^{7} complex with a nearly linear Fe–N–O bond angle. This compound exhibits the highest recorded ν(NO) vibrational frequency for such compounds. Density functional theory studies demonstrate a high degree of β-electron transfer from π^*(NO) to the Fe d orbitals.

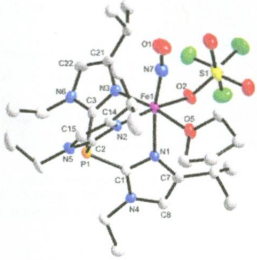

5417 S dx.doi.org/10.1021/ic5006538

Near-IR Photoresponse of Ruthenium Dipyrrinate Terpyridine Sensitizers in the Dye-Sensitized Solar Cells

Guocan Li, Aswani Yella, Douglas G. Brown, Serge I. Gorelsky, Mohammad K. Nazeeruddin, Michael Grätzel,* Curtis P. Berlinguette,* and Michael Shatruk*

The substitution of bidentate dipyrrinate (R-dp) for two NCS^- ligands in the ruthenium black dye leads to strong panchromatic light-harvesting that extends into the near-IR region. The complexes [Ru(tctpy)(R-dp)(NCS)] deposited on a mesoporous TiO_2 electrode afford a measurable incident photon-to-current efficiency up to 950 nm, one of the highest values reported to date for molecular sensitizers in the dye-sensitized solar cell.

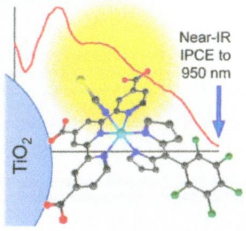

5420 dx.doi.org/10.1021/ic500806n

Fluorescent Naphthalene Diols as Bridging Ligands in Ln^{III} Cluster Chemistry: Synthetic, Structural, Magnetic, and Photophysical Characterization of Ln^{III}_8 "Christmas Stars"

Dimitris I. Alexandropoulos, Adeline Fournet, Luís Cunha-Silva, Andrew M. Mowson, Vlasoula Bekiari, George Christou, and Theocharis C. Stamatatos*

The first use of the fluorescent bridging ligand naphthalene-2,3-diol in 4f-metal coordination chemistry has provided access to a new family of Ln^{III}_8 clusters with a "Christmas-star" topology, single-molecule magnetism behavior, and ligand-centered emissions.

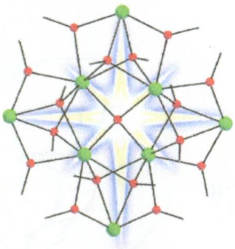

Articles

5423 dx.doi.org/10.1021/ic4030958

Water-Stable Manganese(IV) Complex of a N_2O_4-Donor Non-Schiff-Base Ligand: Synthesis, Structure, and Multifrequency High-Field Electron Paramagnetic Resonance Studies

Malay Dolai, Asma Amjad, Mainak Debnath, Johan van Tol, Enrique del Barco,* and Mahammad Ali*

A novel water-stable mononuclear manganese(IV) complex of a hexacoordinating non-Schiff-base ligand (H_4L) with N_2O_4-donor atoms has been characterized crystallographically and spectroscopically.

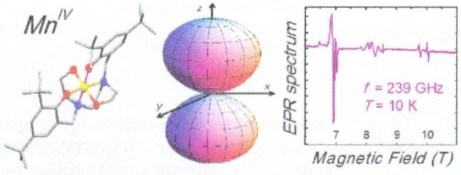

5429 dx.doi.org/10.1021/ic403039x

One-Electron Oxidation Chemistry and Subsequent Reactivity of Diiron Imido Complexes

Subramaniam Kuppuswamy, Tamara M. Powers, Bruce M. Johnson, Carl K. Brozek, Jeremy P. Krogman, Mark W. Bezpalko, Louise A. Berben, Jason M. Keith, Bruce M. Foxman, and Christine M. Thomas*

Upon oxidation, the metal–metal interaction in an $Fe^{II}Fe^{III}$ imido complex is disrupted. This leads to enhanced reactivity of the Fe^{III}–imido fragment toward nitrene transfer. The unique electronic structures of these homobimetallic complexes, which feature two Fe centers in different coordination environments and spin states, is described.

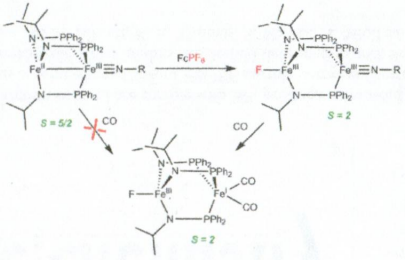

5438 dx.doi.org/10.1021/ic4030603

Synthesis of V/Fe/S Clusters Using Vanadium(III) Thiolate Complexes Bearing a Phenoxide-Based Tridentate Ligand

Nobuhiro Taniyama, Yasuhiro Ohki, and Kazuyuki Tatsumi*

Vanadium(III) thiolate complexes carrying a tridentate (O,P,O) or (O,O,O) ligand were prepared from the reactions of $V(NMe_2)_4$ with the protonated forms of tridentate ligands and thiols. The vanadium–thiolate complexes were found to react with an iron–thiolate complex and elemental sulfur in toluene, leading to the formation of two new V/Fe/S clusters. One of the clusters is structurally relevant to the active site of nickel-dependent CO dehydrogenase.

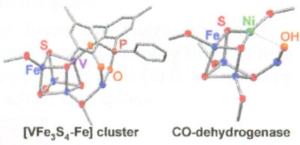

[VFe_3S_4-Fe] cluster CO-dehydrogenase

5447 dx.doi.org/10.1021/ic403074d

Magnetic Properties of 1:2 Mixed Cobalt(II) Salicylaldehyde Schiff-Base Complexes with Pyridine Ligands Carrying High-Spin Carbenes (S_{car} = 2/2, 4/2, 6/2, and 8/2) in Dilute Frozen Solutions: Role of Organic Spin in Heterospin Single-Molecule Magnets

Satoru Karasawa, Kimihiro Nakano, Daisuke Yoshihara, Noriko Yamamoto, Jun-ichi Tanokashira, Takahito Yoshizaki, Yuji Inagaki, and Noboru Koga*

In 1:2 cobalt–carbene complexes Co(*p*-tolsal)$_2$(**CXpy**)$_2$, **X** = **1**, **2**, **3l** (**3b**), and **4**, and Co(*p*-tolsal)$_2$(**cC5py**)$_2$, carbene ferromagnetically interacted with cobalt ion to produce complexes with high-spin ground state, S_{total} = 5/2, 9/2, 13/2 (13/2), and 17/2, exhibiting single-molecule magnet behaviors with U_{eff}/k_B of 40, 65, 73 (72), and 74 K, respectively. On increasing S_{total} from 5/2 to 17/2, the quantum tunneling of magnetization time, τ_Q, increased, while U_{eff}/k_B increased and became constant below and above S_{total} = 13/2, respectively.

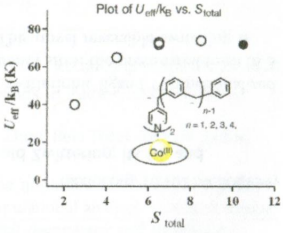

5458 dx.doi.org/10.1021/ic403093r

Disklike Hepta- and Tridecanuclear Cobalt Clusters. Synthesis, Structures, Magnetic Properties, and DFT Calculations

Ji-Dong Leng, Su-Kun Xing, Radovan Herchel,* Jun-Liang Liu, and Ming-Liang Tong*

Two disklike mixed-valence cobalt clusters [$Co^{III}Co^{II}_6$] (**1**) and [$Co^{III}_2Co^{II}_{11}$] (**2**) were successfully isolated. The core structures contain a centered hexagon of a central Co^{III} ion surrounded by a [Co^{II}_6] hexagon for **1** and a larger oligomer based on two vertex-sharing [$Co^{III}Co^{II}_6$] clusters for **2**. Overall ferromagnetic coupling occurs between the Co^{II} ions within both two clusters. The magnetic exchange and magnetic anisotropy was quantified with appropriate spin Hamiltonian models and also supported by DFT calculations.

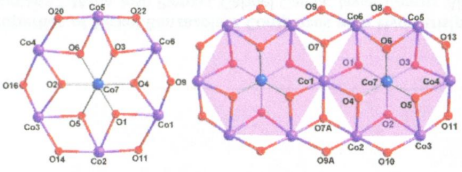

5467 dx.doi.org/10.1021/ic403105q

Internal Versus External Binding of Cationic Porphyrins to Single-Stranded DNA

Abby J. Gaier, Srijana Ghimire, Sarah E. Fix, and David R. McMillin*

Single-stranded DNA hosts internalize the sterically friendly cationic porphyrin Cu(*t*D4) quite effectively, thereby largely blocking access to the copper(II) center, but they do not compare with double-stranded DNA hosts when it comes to binding affinity. Single-stranded hosts are, however, somewhat more competitive at binding the larger, tetrasubstituted analogue Cu(T4), but the binding is external with a low degree of internalization.

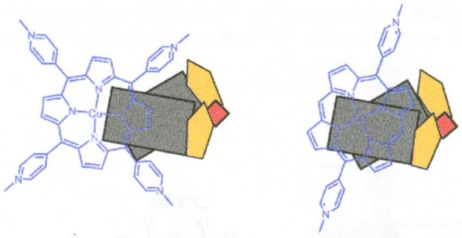

5474 S dx.doi.org/10.1021/ic500108g

Theoretical Study of the Water Oxidation Mechanism with Non-heme Fe(Pytacn) Iron Complexes. Evidence That the $Fe^{IV}(O)$(Pytacn) Species Cannot React with the Water Molecule To Form the O–O Bond

Ferran Acuña-Parés, Miquel Costas, Josep M. Luis,* and Julio Lloret-Fillol*

Computational thermodynamic and kinetic parameters calculated for the O–O bond formation reaction between an N-tetradentate non-heme iron complex with two *cis* labile sites $\{Fe^{IV}(Pytacn)(L)(L')\}^{n+}$ (L = O, L′ = OH, n = 1 or OH_2, n = 2 and L = L′ = OH, n = 2) and water have shown energy barriers (lower $\Delta G^{\ddagger}$ = 28.3 kcal·mol^{-1}) and endergonic reaction energies that are too high to allow the reaction to proceed under experimental conditions ($\Delta G^{\ddagger}_{exp}$ = 17.6 kcal·mol^{-1}). Theoretical oxidation potentials indicate that $Fe^{V}(O)$ ($E°(Fe^{IV/V})$ = 1.69 V) is the higher accessible oxidation state ($E°(Fe^{V/VI})$ = 2.26 V) under catalytic conditions. These results are consistent with the $[Fe^{V}(Pytacn)(O)(OH)]^{2+}$ species as the one directly responsible for the O–O bond formation event in the catalyzed water oxidation through non-heme iron complexes when using cerium(IV) ammonium nitrate as sacrificial oxidant.

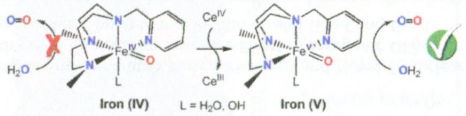

5486 S dx.doi.org/10.1021/ic500114k

Mono- and Diboron Corroles: Factors Controlling Stoichiometry and Hydrolytic Reactivity

Amelia M. Albrett, Kolle E. Thomas, Stefanie Maslek, Anna Młodzianowska, Jeanet Conradie, Christine M. Beavers, Abhik Ghosh,* and Penelope J. Brothers*

The synthesis and structural characterization of a diboryl triaryloctabromocorrole complex fills in a missing link in the family of diboron porphyrinoids. DFT calculations suggest that a strongly electron-withdrawing corrole ligand is required to stabilize the diboryl complex relative to the partially hydrolyzed diboron corrole complexes previously observed. New monoboryl corrole complexes are described, which do not have counterparts in porphyrin chemistry and are stabilized by internal F···H hydrogen bonding.

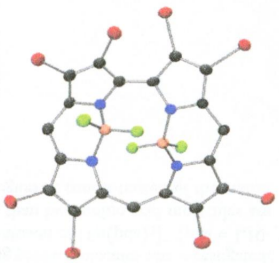

5494 S dx.doi.org/10.1021/ic500101x

$(BMI)_3LnCl_6$ Crystals as Models for the Coordination Environment of $LnCl_3$ (Ln = Sm, Eu, Dy, Er, Yb) in 1-Butyl-3-methylimidazolium Chloride Ionic-Liquid Solution

Yulun Han, Cuikun Lin, Qingguo Meng, Fengrong Dai, Andrew G. Sykes, Mary T. Berry, and P. Stanley May*

Comparison of luminesce spectra and lifetimes of $(BMI)_3LnCl_6$ crystals and $LnCl_3$ dissolved in a BMICl solution suggests that the solution species exhibit a similar octahedral coordination of the Ln^{3+} ions.

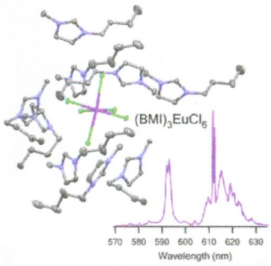

5502 S dx.doi.org/10.1021/ic5001655

Structure and Spectroscopic Properties of Nickel Benzazolate Complexes with Hydrotris(pyrazolyl)borate Ligand

Luisa López-Banet, M. Dolores Santana,* María José Piernas, Gabriel García, Javier Cerezo, Alberto Requena, José Zúñiga,* José Pérez, and Luís García

The syntheses, crystal structures, and spectroscopic absorption properties of pentacoordinate Ni(II) complexes of aromatic N,O-chelate ligands are described, along with density functional theory (DFT) calculations conducted to support them. In addition, the luminescence properties of the complexes in solution and the solid state, and the fluorescent responses observed in the presence of cations of physiological and toxicological importance such as Zn(II), Cd(II), Hg(II), and Cu(II), are also achieved.

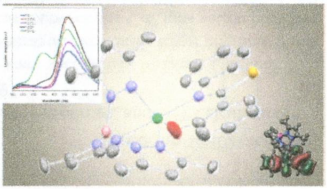

5515 S dx.doi.org/10.1021/ic500194y

Reversible Switching of the Coordination Modes of a Pyridine-Functionalized Quinonoid Zwitterion; Its Di- and Tetranuclear Palladium Complexes

Alessio Ghisolfi, Audrey Waldvogel, Lucie Routaboul, and Pierre Braunstein*

Reversible deprotonation of the N−H groups of the benzoquinonemonoimine core of a zwitterionic ligand N-functionalized by a pyridine donor moiety coordinated to Pd(II) centers allows for the switching of the donor sites: the protonated form in **3** behaves as a N_{Py} donor, whereas in the deprotonated form, N,O chelation leads to **4**. This novel reversible switching is accompanied by a reversible color change of the complexes from red (**3**) to green (**4**).

5527 dx.doi.org/10.1021/ic500196m

Specific Chiral Sensing of Amino Acids Using Induced Circularly Polarized Luminescence of Bis(diimine)dicarboxylic Acid Europium(III) Complexes

Kazuhiro Okutani, Koichi Nozaki, and Munetaka Iwamura*

Induced circularly polarized luminescence (CPL) of rear-earth complexes for chiral-sensing probe molecules was investigated. We found that arginine and histidine induce a CPL signal with much higher intensity in emission of $[Eu(pda)_2]^-$ (pda = 1,10-phenanthroline-2,9-dicarboxylic acid). The concentration dependence revealed that more than two amino acid molecules are involved in the inducement of CPL, which achieves quite high sensitivity in a particular region of concentration of the amino acids ($\sim 10^{-2}$ mol·dm^{-3}).

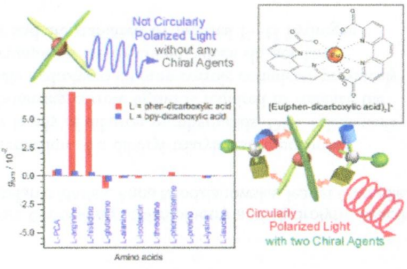

5538 dx.doi.org/10.1021/ic5002144

Photochromic Hybrid Containing *In Situ*-Generated Benzyl Viologen and Novel Trinuclear $[Bi_3Cl_{14}]^{5-}$: Improved Photoresponsive Behavior by the $\pi\cdots\pi$ Interactions and Size Effect of Inorganic Oligomer

Rong-Guang Lin, Gang Xu, Gang Lu, Ming-Sheng Wang, Pei-Xin Li, and Guo-Cong Guo*

Two new viologen metal halide hybrid compounds have been synthesized by an *in situ* solvothermal reaction, and one contains an unprecedented discrete trimer $[Bi_3Cl_{14}]^{5-}$ counterion. Studies on the relationship between structure and photochromic behavior have confirmed that the size of an inorganic oligomer can influence the photoresponsive rate of a viologen dication, and the $\pi\cdots\pi$ interaction may act as not only a powerful factor to stabilize the viologen monocation radical but also the second electron-transfer pathway from a π-conjugated substituent to a viologen cation for a photochromic process.

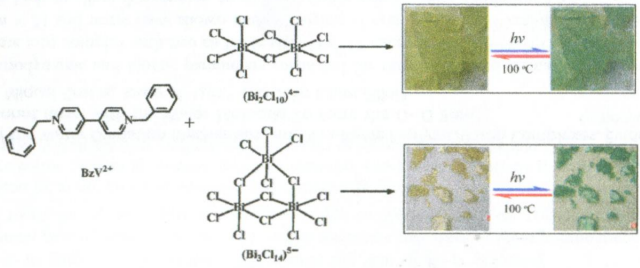

5546 S dx.doi.org/10.1021/ic500226z

[1,2,4]Triazolo[4,3-*a*]Pyridines as Bridging Ligands—Magnetism of Azole-Bridged Dinuclear Copper(II) Complexes Influenced by the Trigonal Distortion Parameter τ

Dominic Kaase, Carla Gotzmann, Stephan Rein, Yanhua Lan, Sylwia Kacprzak,* and Julia Klingele*

With the ligand **L** = 3-(6-methyl-2-pyridyl)-[1,2,4]triazolo[4,3-*a*]pyridine two dinuclear doubly azole-bridged copper(II) complexes $[Cu^{II}_2(\mathbf{L})_2(L')_4](ClO_4)_4$ (L′ = MeCN, **L**) have been prepared. Differing antiferromagnetic coupling strengths have been correlated to dissimilar local geometries about the copper(II) ions. Electron paramagnetic resonance (EPR) spectroscopy and broken-symmetry DFT calculation have been used to investigate the magneto-structural correlations.

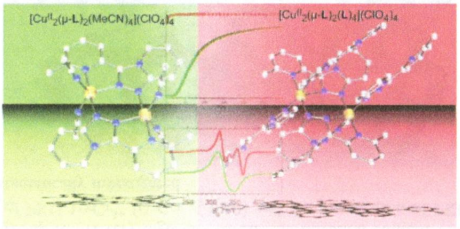

5556 S dx.doi.org/10.1021/ic5002623

Exploring the Noninnocent Character of Electron Rich π-Extended 8-Oxyquinolate Ligands in Ruthenium(II) Bipyridyl Complexes

Stephanie Bellinger-Buckley, Tse-Cing Chang, Seema Bag, David Schweinfurth, Weihong Zhou, Bela Torok, Biprajit Sarkar, Ming-Kang Tsai,* and Jonathan Rochford*

The influence of π-extension and electron rich n $\rightarrow$ π donation has been explored at the noninnocent Ru(dπ)−OQN(π) system using a combination of optical, electrochemical, spectroelectrochemical, and computational analysis. Covalent mixing of the Ru(dπ) atomic and OQN(π) molecular orbitals results in a breakdown of d-orbital degeneracy and significant destabilization of the HOMO level relative to the classic $[Ru(bpy)_3]^{2+}$ system. The potential of this class of ruthenium chromophore in a photovoltaic device is highlighted.

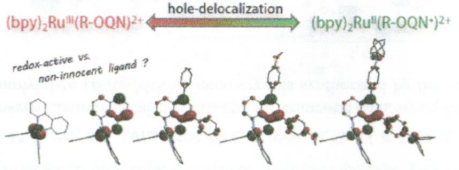

5568 dx.doi.org/10.1021/ic500286v

^{183}W INADEQUATE 2D NMR Spectroscopy of Hetero Arsenato–Phosphato–Tungstate P^V/As^V Substitution in Dawson-Type α-$[As_xP_{2-x}W_{18}O_{62}]^{6-}$ (x = 0–2) and α-$[H_4As_yP_{1-y}W_{18}O_{62}]^{7-}$ (y = 0, 1)

Mohamed Haouas,* Israël-Martyr Mbomekallé,* Neus Vila, Pedro de Oliveira, and Francis Taulelle

The synthesis and NMR characterization of the Dawson-type arsenato–phosphato–tungstate α-$[AsPW_{18}O_{62}]^{6-}$ is reported. 2-D NMR ^{183}W INADEQUATE experiments were employed to fully assign resonances and determine precisely NMR parameters, including $^2J_{W-O-W}$ scalar couplings. A systematic comparative NMR study with the four phosphorus- and arsenic-based Dawson compounds, i.e., the symmetric α-$[X_2W_{18}O_{62}]^{6-}$ and unsymmetric α-$[H_4XW_{18}O_{62}]^{7-}$ for X = P^V, As^V, was conducted to investigate the effect of P/As substitutions on the NMR observables $\delta_{W\text{-}183}$, $\delta_{P\text{-}31}$, $^2J_{W-O-W}$, and $^2J_{W-O-P}$.

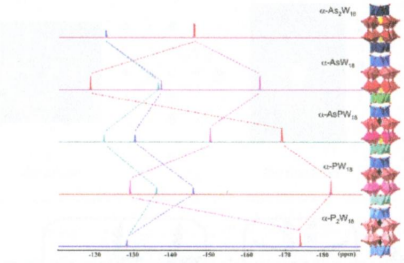

5575 dx.doi.org/10.1021/ic500291v

Electron-Deficient Telluride $Cs_3Cu_{20}Te_{13}$ with Sodalite-Type Network: Syntheses, Structures, and Physical Properties

Wen-Juan Huai, Jin-Ni Shen, Hua Lin, Ling Chen, and Li-Ming Wu*

The first sodalite-type telluride, $Cs_3Cu_{20}Te_{13}$, is discovered. DFT analysis uncovers the unique feature of the p-type metallic sodalite framework accommodating anionic guest species, which agrees with the experimental metallic electrical conductivity and Pauli paramagnetism.

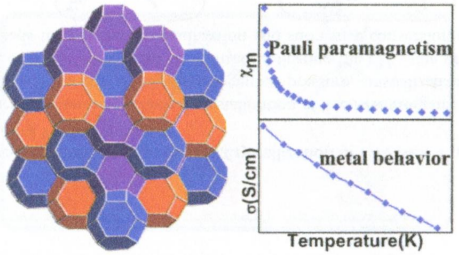

5581 S dx.doi.org/10.1021/ic500306y

From 1D Helix to 0D Loop: Nitrite Anion Induced Structural Transformation Associated with Unexpected *N*-Nitrosation of Amine Ligand

Jing-Yun Wu,* Yu-Chiao Liu, and Tzu-Ching Chao

Nitrite anion induced structural transformation from 1D helix to 0D molecular loop associated with in situ *N*-nitrosation of amine ligand is observed for the first time.

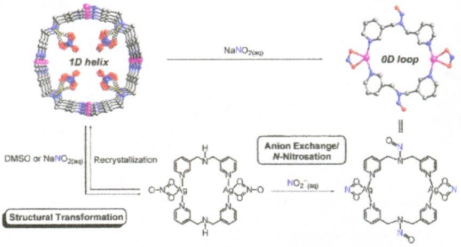

5589 S dx.doi.org/10.1021/ic500335x

Experimental and Theoretical Investigations of Electronic Structure and Photoluminescence Properties of β-Ag_2MoO_4 Microcrystals

A. F. Gouveia, J. C. Sczancoski, M. M. Ferrer, A. S. Lima, M. R. M. C. Santos, M. Siu Li, R. S. Santos, E. Longo, and L. S. Cavalcante*

By investigating a correlation between theoretical calculations and experimental data, an explanation of the electronic structure and optical properties of silver molybdate (β-Ag_2MoO_4) microcrystals synthesized by the microwave-assisted hydrothermal method is sought.

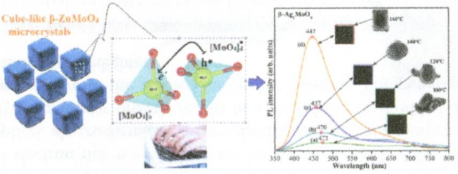

5600 S dx.doi.org/10.1021/ic500352g

Systematic Study of Cr^{3+} Substitution into Octahedra-Based Microporous Aluminoborates

Qiaoqi Li, Cong Lin, Zhengyang Zhou, Jing Ju, Guobao Li, Jianhua Lin, Wenliang Gao, Rihong Cong,* and Tao Yang*

Single crystals of pure aluminoborate PKU-1 ($Al_3B_6O_{12}(OH)_5 \cdot nH_2O$) were obtained, and the structure was redetermined to be nonsymmetryic in the space group *R*3. A very high Cr^{3+}-to-Al^{3+} substitution content (~50 atom %) in PKU-1 can be achieved. The thermal behavior of PKU-1:xCr^{3+} ($0 \le x \le 0.50$) and the preparation of PKU-5:xCr^{3+} ($0.04 \le x \le 0.20$) by thermal decomposition were systematically investigated.

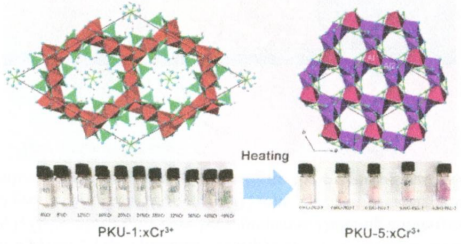

5609 S dx.doi.org/10.1021/ic500278y

Localization and Impact of Pb-Non-Bonded Electronic Pair on the Crystal and Electronic Structure of Pb_2YSbO_6

Sebastián A. Larrégola,* José A. Alonso, Victor A. de la Peña-O'Shea, Denis Sheptyakov, Vladimir Pomjakushin, María T. Fernandez-Díaz, and José C. Pedregosa

Pb_2YSbO_6 perovskite shows two consecutive phase transitions. The RT phase shows a highly distorted crystal structure, mainly related to strong stereoactivity of the nonbonded electronic pair of lead atoms. Moreover, the thermal evolution shows a transition from this structure to an incommensurate phase with a thermal independent propagation vector. The thermal evolution ends in a cubic double perovskite characterized by the presence of an atomic static disorder of lead atoms.

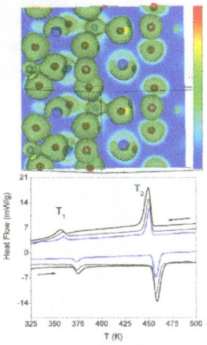

5619 S dx.doi.org/10.1021/ic500369m

Influence of the Synthesis Parameters onto Nucleation and Crystallization of Five New Tin–Sulfur Containing Compounds

Jessica Hilbert, Christian Näther, and Wolfgang Bensch*

The distinct control of the syntheses parameters achieved crystallization of five new inorganic–organic hybrid tin sulfides with 1,10-phenathroline as the organic component. At higher autogenous pressure, crystallization and conversion of several compounds are suppressed, and only one compound crystallized. Adjusting the pH value of the solution, the concentration, and the volume of the solvent leads to sequential crystallization and successive conversion of the compounds.

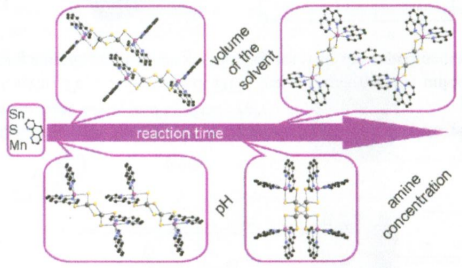

5631 dx.doi.org/10.1021/ic500404z

Pillared-Layer Cluster Organic Frameworks Constructed from Nanoscale Ln_{10} and Cu_{16} Clusters

Wei-Hui Fang and Guo-Yu Yang*

Two pillared-layer cluster organic frameworks, $[Ln_5(\mu_3\text{-}OH)_4(\mu\text{-}H_2O)Cu_8I_8L_{11}]\cdot H_2O$ (L = 4-pyridin-4-yl-benzoate; Ln = Dy **1**, Eu **2**), have been made under hydrothermal conditions, in which the $[Dy_{10}(\mu_3\text{-}OH)_8]^{22+}$ cluster organic networks are pillared by the L−$[Cu_{16}I_{16}]$−L complexes to form 3D cluster organic frameworks, showing an intriguing example of binodal (8,14)-connected net.

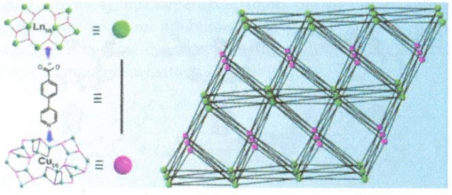

5637 dx.doi.org/10.1021/ic500408j

Controlling Ground and Excited State Properties through Ligand Changes in Ruthenium Polypyridyl Complexes

Dennis L. Ashford, Christopher R. K. Glasson, Michael R. Norris, Javier J. Concepcion, Shahar Keinan, M. Kyle Brennaman, Joseph L. Templeton, and Thomas J. Meyer*

The synthesis and photophysical analysis of nine new Ru^{II} polypyridyl complexes of the form $[Ru(bpy)_2(N{-}N)]^{2+}$, where N−N is bidentate polypyridyl ligand, is described. Variations in the ground state and exited state redox potentials as a function of the π^* acceptor levels in the N−N ligand is featured.

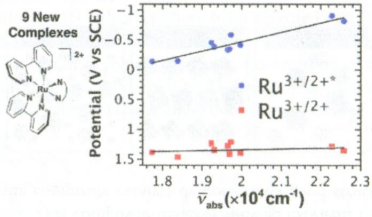

5647 dx.doi.org/10.1021/ic5004098

Cationic Copper(II)-containing Surfactants: Molecular Structures, Film Morphology, and Influence on the Alignment of Nematic Mesogens

Cláudio N. Verani,* Jeffery Driscoll, Paul H. Keyes, and Mary Jane Heeg

New cationic copper(II)-containing surfactants were synthesized and characterized and were investigated at the air/water interface and on solid surfaces where they influence the alignment of nematic mesogens.

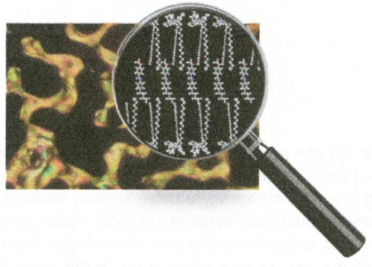

5656 dx.doi.org/10.1021/ic500416s

Dense Si_xGe_{1-x} ($0 < x < 1$) Materials Landscape Using Extreme Conditions and Precession Electron Diffraction

George Serghiou,* Gang Ji, Monika Koch-Müller, Nicholas Odling, Hans J. Reichmann, Jonathan P. Wright, and Paul Johnson

Pressure gently tunes to radically transforms matter, making it formidable in developing targeted materials and materials landscapes. Crystals may initially be small and sparsely populated within complex agglomerates. X-ray and electron diffraction offer complementing angular and spatial resolution. Precession improves electron diffraction intensities, strengthening single crystal assignment. We develop a dense SiGe landscape by heating Si and Ge at pressures where they undergo phase transitions, transform to metals and their melting points converge. Distinctive precession electron diffraction patterns are shown.

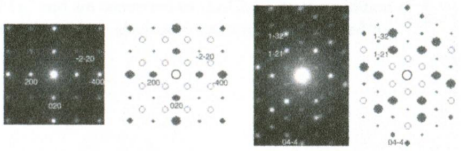

5663 dx.doi.org/10.1021/ic500425c

Synthesis and Characterization of Multinuclear Manganese-Containing Tungstosilicates

Rami Al-Oweini, Bassem S. Bassil, Jochen Friedl, Veronika Kottisch, Masooma Ibrahim, Marie Asano, Bineta Keita, Ghenadie Novitchi, Yanhua Lan, Annie Powell, Ulrich Stimming, and Ulrich Kortz*

We prepared several high- and mixed-valent Mn-containing polyoxometalates of the Keggin type, $[Mn^{II}_3(OH)_3(H_2O)_3(A\text{-}\alpha\text{-}SiW_9O_{34})]^{7-}$ (**1**), $[Mn^{III}_3(OH)_3(H_2O)_3(A\text{-}\alpha\text{-}SiW_9O_{34})]^{4-}$ (**2**), $[Mn^{III}_3(OH)_3(H_2O)_3(A\text{-}\beta\text{-}SiW_9O_{34})]^{4-}$ (**3**), $[Mn^{III}_3Mn^{IV}O_3(CH_3COO)_3(A\text{-}\alpha\text{-}SiW_9O_{34})]^{6-}$ (**4**), and $[Mn^{III}_3Mn^{IV}O_3(CH_3COO)_3(A\text{-}\beta\text{-}SiW_9O_{34})]^{6-}$ (**5**). Magnetic and electrochemical studies confirmed the compositions and structures of **1**–**5**, and the latter technique revealed exciting redox properties. The manganese–oxo clusters in polyanions **4** and **5** exhibit similar structural features as the active site of photosystem II.

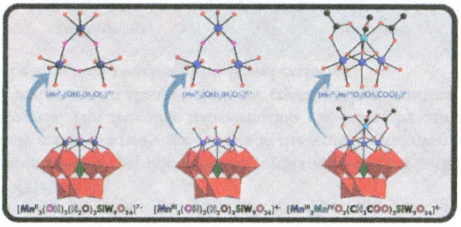

5674 dx.doi.org/10.1021/ic500443t

Synthesis, Crystal Structure, and Magnetic Characterization of the Three-Dimensional Compound $[Co_2(cbut)(H_2O)_3]_n$ (H_4cbut = 1,2,3,4-Cyclobutanetetracarboxylic Acid)

Pau Díaz-Gallifa, Oscar Fabelo,* Jorge Pasán,* Laura Cañadillas-Delgado, Juan Rodríguez-Carvajal, Francesc Lloret, Miguel Julve, and Catalina Ruiz-Pérez

The crystal structure and magnetic properties of a new metal–organic framework of formula $[Co_2(cbut)(H_2O)_3]_n$, have been characterized by combining synchrotron radiation, neutron diffraction and magnetometry measurements. The 3D compound exhibits a field-induced ferromagnetic phase transition under dc magnetic fields above 1500 G and an antiferromagnetic ordering at temperatures below 5.0 K, the magnetic structure of the antiferromagnetic phase being determined by neutron diffraction at 2.0 K

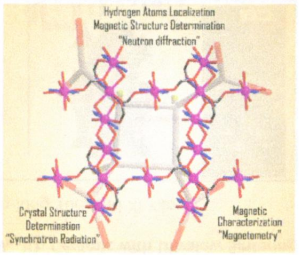

5684 S dx.doi.org/10.1021/ic500437k

Layered Compounds $BaM_2Ge_4Ch_6$ (M = Rh, Ir and Ch = S, Se) with Pyrite-Type Building Blocks and Ge−Ch Heteromolecule-Like Anions

Hechang Lei, Jun-ichi Yamaura, Jiangang Guo, Yanpeng Qi, Yoshitake Toda, and Hideo Hosono*

The layered compounds $BaM_2Ge_4Ch_6$ (M = Rh, Ir; Ch = S, Se) with M−Ge−Ch pyrite-type building units were synthesized using high-pressure and high-temperature methods. Theoretical calculations and experimental results indicate that there are strongly polarized covalent bonds between the Ge and Ch atoms, forming heteromolecule-like anions in these compounds. Moreover, Ge atoms in this structure exhibit an unusual valence state (~+1) due to the tetrahedral coordination environment of Ge atoms along with M and Ch atoms simultaneously.

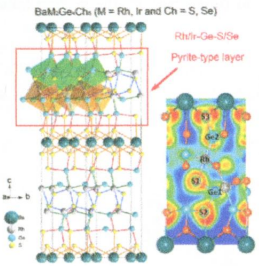

5692 S dx.doi.org/10.1021/ic500464v

Monodispersed Ag Nanoparticles as Catalyst: Preparation Based on Crystalline Supramolecular Hybrid of Decamethylcucurbit[5]uril and Silver Ions

Hong-Fang Li, Jian Lü, Jing-Xiang Lin, and Rong Cao*

Monodispersed silver nanoparticles (Ag^0 NPs) have been first prepared on the basis of a postsynthesis from the new crystalline supramolecular hybrid solid $\{[Ag(H_2O)]_2(H_2O@Me_{10}CB[5])\}\cdot 2NO_3\cdot 2H_2O$, assembled from Ag^+ ions and decamethylcucurbit[5]uril ($Me_{10}CB[5]$). This composite material showed excellent catalytic performance for the reduction reactions of nitrophenols. Moreover, the composite catalyst demonstrated good structural stability and reusability in consecutive cycles.

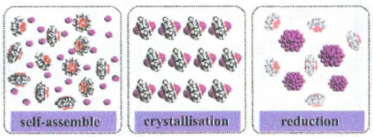

5698 S dx.doi.org/10.1021/ic500471w

Synthesis and Lanthanide Coordination Chemistry of Phosphine Oxide Decorated Dibenzothiophene and Dibenzothiophene Sulfone Platforms

Daniel Rosario-Amorin, Sabrina Ouizem, Diane A. Dickie, Robert T. Paine,* Roger E. Cramer, Benjamin P. Hay, Julien Podair, and Lætitia H. Delmau

Syntheses of neutral multifunctional ligands based upon dibenzothiophene and dibenzothiophene sulfone platforms decorated with phosphine oxide and methyl phosphine oxide donors are described. Low steric strain energy metal chelating binding conditions are identified, and selected coordination chemistry with lanthanide(III) cations is outlined.

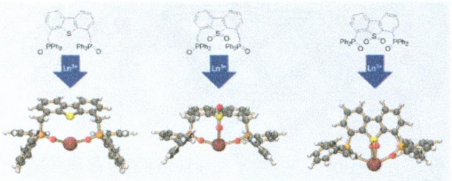

5712 dx.doi.org/10.1021/ic5004808

Structure, Phase Evolution, and Microwave Dielectric Properties of $(Ag_{0.5}Bi_{0.5})(Mo_{0.5}W_{0.5})O_4$ Ceramic with Ultralow Sintering Temperature

Di Zhou,* Wen-Bo Li, Jing Guo, Li-Xia Pang, Ze-Ming Qi, Tao Shao, Hui-Dong Xie, Zhen-Xing Yue, and Xi Yao

The scheelite structure $(Ag_{0.5}Bi_{0.5})(Mo_{0.5}W_{0.5})O_4$ ceramic can be well sintered at 580 °C with permittivity ~26.3, Q_f value ~10000 GHz, and temperature coefficient ~+20 ppm/°C. Its good microwave dielectric properties and chemical compatibility with Al make it a candidate for low-temperature cofired ceramics technology.

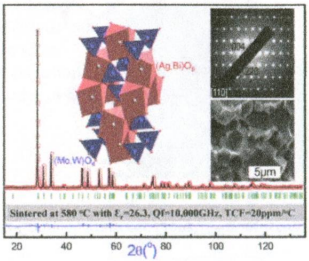

5717 dx.doi.org/10.1021/ic500478p

Concerted Ligand Exchange and the Roles of Counter Anions in the Reversible Structural Switching of Crystalline Peptide Metallo-Macrocycles

Ryosuke Miyake* and Mitsuhiko Shionoya

Reversible crystal-to-crystal transformations in peptide Ni^{II} macrocycles were studied in detail using structural and thermodynamic analyses. The study revealed a two-stage process in the structural transformation accompanied by concerted ligand exchange within one macrocycle. This reversible transformation was caused by compensation for the large degree of stabilization due to water uptake and structural changes. Both the crystal packing structure and the types of counter anions were key factors that facilitated the structural switching with ligand exchange.

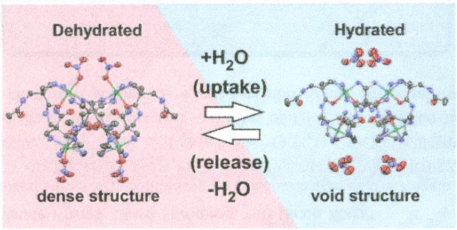

5724 dx.doi.org/10.1021/ic500483p

Antitumoral, Antihypertensive, Antimicrobial, and Antioxidant Effects of an Octanuclear Copper(II)-Telmisartan Complex with an Hydrophobic Nanometer Hole

María S. Islas, Juan J. Martínez Medina, Libertad L. López Tévez, Teófilo Rojo, Luis Lezama, Mercedes Griera Merino, Laura Calleros, María A. Cortes, Manuel Rodriguez Puyol, Gustavo A. Echeverría, Oscar E. Piro, Evelina G. Ferrer, and Patricia A. M. Williams*

A porous coordination compound from telmisartan with Cu(II) with nanochannels has been successfully synthesized. The complex exhibits selective scavenging activity against superoxide anion and significant inhibition of the *Staphylococcus aureus* bacterial strain. The Cu-telmisartan complex produces inhibition of the viability of lung and prostate cancer cells. An apoptotic mechanism of action has been determined by flow cytometry for the high cytotoxic LNCaP cell line. The antihypertensive effect of telmisartan was retained upon complex formation.

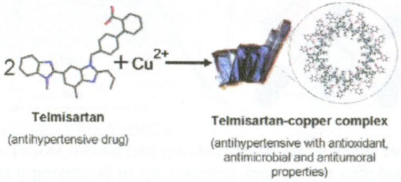

5738 dx.doi.org/10.1021/ic500555w

Platinum(II) Complexes of N^C^N-Coordinating 1,3-Bis(2-pyridyl)benzene Ligands: Thiolate Coligands Lead to Strong Red Luminescence from Charge-Transfer States

William A. Tarran, Gemma R. Freeman, Lisa Murphy, Adam M. Benham, Ritu Kataky, and J. A. Gareth Williams*

A family of 10 new cyclometalated platinum(II) complexes have been prepared that incorporate a cyclometalating tridentate ligand together with a monodentate thiolate ligand. The complexes are phosphorescent in solution at room temperature. In comparison to the parent complexes containing a chloride coligand, the emission of the thiolate complexes is strongly red-shifted, increasingly so with the electron richness of the thiolate. Electrochemical data and TD-DFT calculations indicate that the change is due to the introduction of a charge-transfer state, but nitro-substituted thiolates behave differently.

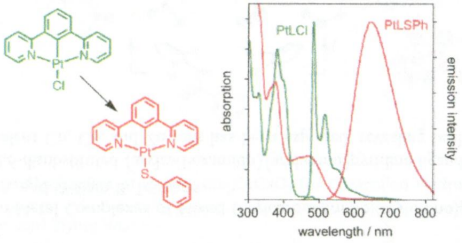

5750 dx.doi.org/10.1021/ic5005616

An Electrochemical and Spectroscopic Study of Nd(III) and Pr(III) Coordination in the 1-Butyl-1-methylpyrrolidinium Bis(trifluoromethylsulfonyl)imide Ionic Liquid Containing Chloride Ion

Li-Hsien Chou and Charles L. Hussey*

The coordination and accessible oxidation states of Nd and Pr ions in the room-temperature ionic liquid, 1-butyl-1-methylpyrrolidinium bis(trifluoromethylsulfonyl)-imide (BuMePyroTf_2N), were investigated by electronic absorption spectroscopy, cyclic staircase voltammetry, and controlled potential coulometry before and after the addition of chloride ion as BuMePyroCl. Trivalent $[Ln(Tf_2N)_x]^{(x-3)-}$ species are produced by anodic oxidation of Ln^0 and are converted to $[LnCl_6]^{3-}$ by the addition of Cl^-. Hypersensitive and pseudohypersensitive electronic transitions were noted for Nd^{3+} and Pr^{3+}, respectively.

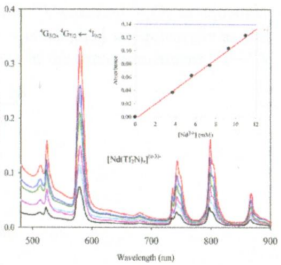

5759 dx.doi.org/10.1021/ic500544n

Ligand Effects on the Structure and Magnetic Properties of Alternating Copper(II) Chains with 2,2′-Bipyrimidine- and Polymethyl-Substituted Pyrazolates as Bridging Ligands

Isabel Castro,* M. Luisa Calatayud, Wdeson P. Barros, José Carranza, Miguel Julve, Francesc Lloret, Nadia Marino,* and Giovanni De Munno

The solid-state aggregation of antiferromagnetically coupled, mono- or bis(pyrazolate)(aqua/hydroxo)-bridged dicopper(II) complexes through bis-bidentate 2,2′-bipyrimidine leads to two different types of copper(II) chains with regular alternating intrachain antiferromagnetic interactions.

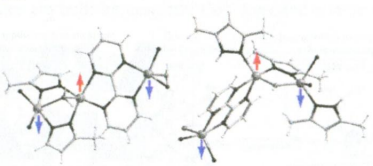

5772 dx.doi.org/10.1021/ic5006314

Experimental and Theoretical Approaches to Redox Innocence of Ligands in Uranyl Complexes: What Is Formal Oxidation State of Uranium in Reductant of Uranyl(VI)?

Koichiro Takao,* Satoru Tsushima, Toshinari Ogura, Taro Tsubomura, and Yasuhisa Ikeda

The *noninnocent* ligand system for uranyl(VI) was fully demonstrated for the first time by both experimental and theoretical approaches.

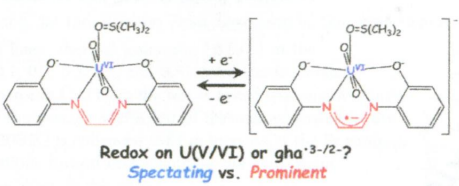

5781 S dx.doi.org/10.1021/ic500635q

Photochemical Reactivity of the Iron(III) Complex of a Mixed-Donor, α-Hydroxy Acid-Containing Chelate and Its Biological Relevance to Photoactive Marine Siderophores

Jennifer E. Grabo, Mark A. Chrisman, Lindsay M. Webb, and Michael J. Baldwin*

Irradiation of the Fe(III) complex of a tetradentate salicylidene-α-hydroxy acid chelate gives different products in air than under Ar. After a common initial photochemical event, additional light-dependent and non-light-dependent steps result in further cleavage of the chelate in air. Understanding these reaction sequences sheds light on the differences in photochemical reaction products observed for different natural marine siderophores.

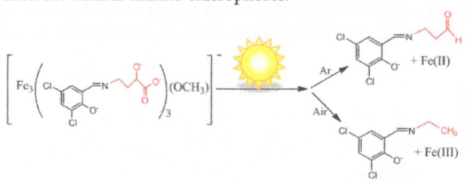

5788 S dx.doi.org/10.1021/ic500638z

Linkage Isomerism in Transition-Metal Complexes of Mixed (Arylcarboxamido)(arylimino)pyridine Ligands

David W. Boyce, Debra J. Salmon, and William B. Tolman*

A modular synthesis of hybrid 2,6-disubstituted (arylcarboxamido)(arylimino)pyridine ligands has been developed, and their coordination chemistry with divalent Cu, Co, and Zn ions has been explored, revealing both *N,N′,N″*- and *O,N,N′*-binding.

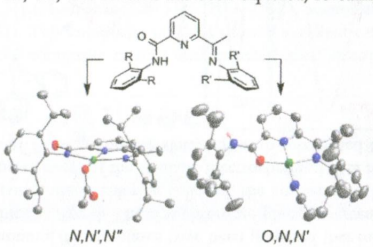

5797 dx.doi.org/10.1021/ic5006133

Structural and Mechanical Properties of Platinum Carbide

Qian Li, Xinxin Zhang, Hanyu Liu, Hui Wang,* Miao Zhang, Quan Li,* and Yanming Ma

The current calculations reveal that the synthesized PtC has a zinc blende structure at ambient conditions and the position of carbon atoms in PtC are not fixed and fluctuating in the platinum sublattice at high-pressure conditions. The theoretical Poisson's ratio and elastic anisotropic factors suggest that the synthesized PtC is highly anisotropic and strongly dependent on the crystallographic direction.

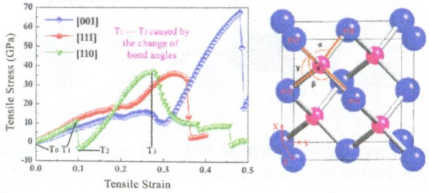

5803 S

dx.doi.org/10.1021/ic500615k

Widely Applicable Metallacarborane Reagents for π-Conjugated Systems

Pau Farràs, Ana D. Musteti, Isabel Rojo, Clara Viñas, Francesc Teixidor,* and Mark E. Light

A series of new starting materials bearing a cobaltabisdicarbollide were synthesized with the ability to generate extended π-conjugated systems, considering also the metallacarborane a pseudoaromatic unit. The lack of these reagents prompted us to synthesize compounds having terminal formyl and vinyl functional groups that can react further by well-developed organic chemistry reactions.

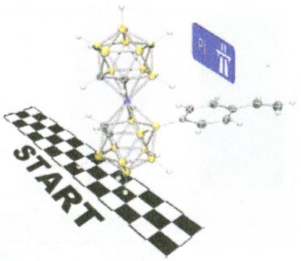

5810 S

dx.doi.org/10.1021/ic500663x

Fe^{III} Bipyrrolidine Phenoxide Complexes and Their Oxidized Analogues

Linus Chiang, Didier Savard, Yuichi Shimazaki, Fabrice Thomas, and Tim Storr*

Symmetric (FeL^1Cl) and dissymmetric (FeL^2Cl_2) Fe^{III} complexes employing a chiral bipyrrolidine backbone were prepared, and their one-electron oxidized forms were investigated in solution by experimental (electrochemistry, UV−vis-NIR, resonance Raman and electron paramagnetic resonance spectroscopies) and theoretical (density functional theory) means. Both FeL^1Cl and FeL^2Cl_2 contain a redox active phenoxide moiety, which was shown to be the locus of oxidation.

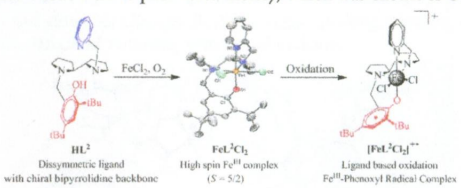

5820 S

dx.doi.org/10.1021/ic500651r

New Evidence in an Old Case: The Question of Chromium Hexafluoride Reinvestigated

Tobias Schlöder, Felix Brosi, Benjamin J. Freyh, Thomas Vent-Schmidt, and Sebastian Riedel*

The question of the existence of chromium hexafluoride has been reinvestigated in new matrix isolation experiments as well as by quantum-chemical calculations at the ab initio level. The bands of the Cr_2F_{10} dimer could be assigned in the spectra, and the calculations suggest CrF_6 to be thermochemically instable. Together, these results give conclusive evidence that the debated IR absorption must be assigned to chromium pentafluoride. However, the formation of CrF_6 at high fluorine pressures cannot be excluded.

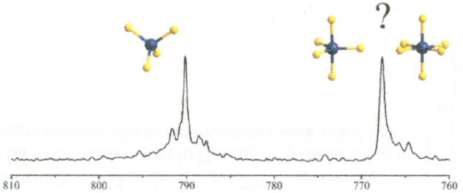

5830 dx.doi.org/10.1021/ic500706f

Crystal Structure, Physical Properties, and Electronic and Magnetic Structure of the Spin $S = {}^5/_2$ Zigzag Chain Compound $Bi_2Fe(SeO_3)_2OCl_3$

Peter S. Berdonosov,* Elena S. Kuznetsova, Valery A. Dolgikh, Alexei V. Sobolev, Igor A. Presniakov, Andrei V. Olenev, Badiur Rahaman, Tanusri Saha-Dasgupta, Konstantin V. Zakharov, Elena A. Zvereva, Olga S. Volkova, and Alexander N. Vasiliev

The isolated set of spin $S = {}^5/_2$ zigzag chains of corner-sharing FeO_6 octahedrons in the crystal structure of the new bismuth iron selenite oxochloride $Bi_2Fe(SeO_3)_2OCl_3$ is responsible for the quasi-one-dimensional nature of magnetism in this compound.

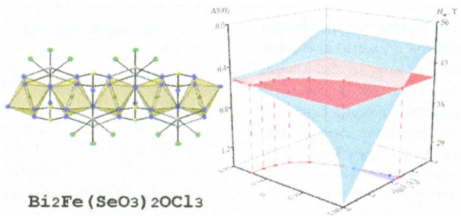

5839 dx.doi.org/10.1021/ic500724q

Crown Ether Complexes of Uranyl, Neptunyl, and Plutonyl: Hydration Differentiates Inclusion versus Outer Coordination

Yu Gong and John K. Gibson*

Gas-phase complexes of uranyl, neptunyl, and plutonyl with 3*N*-Crown-*N* (N = 4, 5, or 6) were produced by electrospray ionization. Structures of 1:1 actinyl–crown complexes are deduced from hydration, which requires that the actinide be exposed for association with water: hydration occurs for outer-coordination isomers but not for inclusion isomers. Hydration indicates inclusion actinyl–18C6 complexes, outer-coordination actinyl–12C4 complexes, and both isomers for actinyl–15C5 complexes, depending on the route to formation.

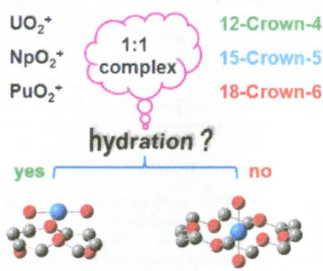

5845 dx.doi.org/10.1021/ic500747x

Understanding the Crystallization Mechanism of Delafossite $CuGaO_2$ for Controlled Hydrothermal Synthesis of Nanoparticles and Nanoplates

Mingzhe Yu, Thomas I. Draskovic, and Yiying Wu*

Synthesis of delafossite $CuGaO_2$ under low-temperature (<250°C) hydrothermal conditions requires the stabilization of Cu^I cations in aqueous solution and the controlling of the hydrolysis of Ga^{III} species. The oriented attachment (OA) growth is proposed as the crystal growth mechanism to explain the formation of large $CuGaO_2$ nanoplates. Importantly, by suppressing this OA process, delafossite $CuGaO_2$ nanoparticles of a 20 nm size were successfully synthesized for the first time.

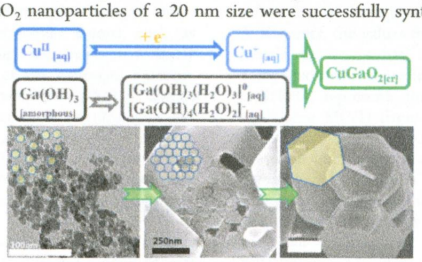

5852 Ⓢ dx.doi.org/10.1021/ic500787v

Dinuclear $[(V^{V}O(putrebactin))_2(\mu\text{-}OCH_3)_2]$ Formed in Solution as Established from LC-MS Measurements Using ^{50}V-Enriched V_2O_5

Cho Zin Soe, Amalie A. H. Pakchung, and Rachel Codd*

The reaction between the macrocyclic dihydroxamic acid siderophore putrebactin and 36% ^{50}V-enriched V_2O_5 in aqueous methanol formed $[(V^{V}O(putrebactin))_2(\mu\text{-}OCH_3)_2]$ ($[M + Na^+]^+$, m/z_{calc} 959.3), which was assigned unequivocally as the dinuclear species from the mass spectrum isotope pattern, which presented as the composite of the three constituent ^{51}V–^{51}V (41.0%), ^{51}V–^{50}V (46.1%), and ^{50}V–^{50}V (12.9%) species.

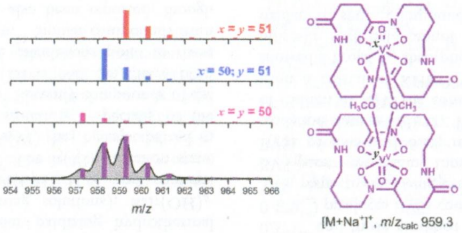

5862 Ⓢ dx.doi.org/10.1021/ic500793z

Syntheses and Magnetic Properties of New Tellurite–Sulfate Compounds $M_2(TeO_3)(SO_4)\cdot H_2O$ (M = Co, Mn) with a Layer Structure Showing a Distorted Honeycomb Spin–Lattice

Yingying Tang, Zhangzhen He,* Wenbin Guo, Suyun Zhang, and Ming Yang

A new tellurite–sulfate $Co_2(TeO_3)(SO_4)\cdot H_2O$ exhibits unique structural and magnetic features, in which the wavelike layers with a distorted honeycomb spin–lattice are built by magnetic Co^{2+} ions and a large spin-canted behavior is observed.

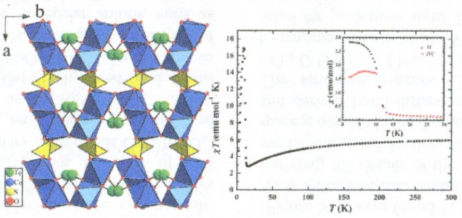

5869 Ⓢ dx.doi.org/10.1021/ic500801b

Enhanced Negative Thermal Expansion in $La_{1-x}Pr_xFe_{10.7}Co_{0.8}Si_{1.5}$ Compounds by Doping the Magnetic Rare-Earth Element Praseodymium

Wen Li, Rongjin Huang,* Wei Wang, Jie Tan, Yuqiang Zhao, Shaopeng Li, Chuanjun Huang, Jun Shen, and Laifeng Li*

The temperature dependence of linear thermal expansion ($\Delta L/L$) in the $La_{1-x}Pr_xFe_{10.7}Co_{0.8}Si_{1.5}$ (x = 0, 0.1, 0.2, 0.3, 0.4, and 0.5) compounds shows pronounced negative thermal expansion (NTE) in the whole tested temperature range. Moreover, the absolute value of the average coefficient of thermal expansion in the NTE temperature region (200–300 K) is enhanced with an increase of the Pr content. The work has significant implications toward understanding the Pr element contribution and magnetovolume effect in this series.

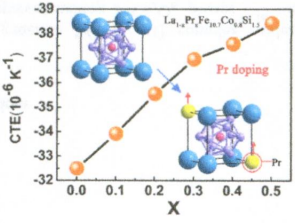

Ⓢ Supporting Information available via online article